Available online at www.sciencedirect.com

SciVerse ScienceDirect

Scripta Materialia 68 (2013) 563–566

Scripta MATERIALIA

www.elsevier.com/locate/scriptamat

Atom-probe tomographic study of γ/γ′ interfaces and compositions in an aged Co–Al–W superalloy

Peter J. Bocchini,[a,*] Eric A. Lass,[b] Kil-Won Moon,[b] Maureen E. Williams,[b] Carelyn E. Campbell,[b] Ursula R. Kattner,[b] David C. Dunand[a,b] and David N. Seidman[a,c]

[a] *Department of Materials Science and Engineering, Northwestern University, 2220 Campus Drive, Evanston, IL 60208-3108, USA*
[b] *National Institute of Standards and Technology, Metallurgy Division, Gaithersburg, MD 20899-8555, USA*
[c] *Northwestern University Center for Atom-Probe Tomography (NUCAPT), 2220 Campus Drive, Evanston, IL 60208-3108, USA*

Received 8 August 2012; revised 13 November 2012; accepted 27 November 2012
Available online 12 December 2012

Atom-probe tomography (APT) is utilized to investigate, in a Co–9.7Al–10.8W at.% alloy aged at 900 °C for ~1000 h, the phase compositions and partitioning behavior of the two-phase γ(face-centered cubic)/γ′($L1_2$) microstructure. The APT composition of the γ-matrix (Co–8.97Al–5.69W at.%) agrees well with a previously reported measurement made by energy-dispersive X-ray spectroscopy; however, the composition of the γ′($L1_2$) precipitates (Co–10.03Al–12.48W at.%) is slightly richer in W and Al, and leaner in Co. Partitioning coefficients and Al interfacial excesses are also calculated.

Keywords: Cobalt alloys; Superalloy; Atom-probe tomography; Intermetallic compounds; Interfaces

Nickel-based superalloys owe their excellent strength at ambient and elevated temperatures to their two-phase γ (face-centered cubic, fcc)/γ′ ($L1_2$) microstructure consisting of coherent γ′-Ni_3Al-based precipitates in a disordered fcc γ-Ni–Al based matrix [1–4]. Until recently, it was believed that analogous Co-based γ/γ′ structures did not exist, thus relegating Co-based alloys to applications at moderate temperatures and stresses. In 2006, Sato et al. discovered in the Co–Al–W ternary system a γ(fcc)/γ′($L1_2$) microstructure analogous to that of Ni-based superalloys [5]. The Co–Al–W phase diagram presented by Sato et al. [5] shows that, at 900 °C, the γ/γ′ two-phase region is significantly narrower than in the Ni–Cr–Al phase diagram, stressing the importance of knowing the exact compositions of both phases, lest the Co–Al–W alloy deviates to one of the surrounding three-phase field regions with embrittling phases. High-temperature flow-stress [6,7] and creep measurements [8–10] of the γ/γ′ Co–Al–W superalloys with quaternary and higher alloying additions have shown promise for continued development for high-temperature applications. Due to the rather limited literature available on the Co–Al–W system, further validation is necessary to better characterize this phase diagram at equilibrium and the microstructural evolution including the evolution of the γ- and γ′-phase compositions during nucleation, growth and coarsening. Understanding the evolution of these phases is essential as they exhibit strong deviations from their equilibrium values in γ/γ′ Ni–Cr–Al superalloys [11,12]. To date, very few compositional measurements have been reported in the literature. The original phase diagram proposed by Sato et al. remains the standard, and few additional reports exist on characterizing the Co–Al–W phase diagram. Some have measured the γ-compositions in multi-phase systems but have not reported the γ′-compositions due to questions concerning phase stability [13,14], while others have attempted to cast single-phase γ′-ingots to study the mechanical properties of the $L1_2$ phase [15–18]. Of all the single-phase γ′-alloys, Co–10Al–11W at.% was the only composition investigated that did not contain secondary phases. Recently, Meher et al. [19] used atom-probe tomography (APT) to measure the composition of a ternary Co alloy at 765 °C; additional investigation is, however, necessary to further develop the phase diagram of this promising new class of Co-based alloys.

Herein, the nanostructure of a homogenized and aged Co–Al–W ternary alloy is examined utilizing an ultraviolet laser-assisted local-electrode atom-probe (LEAP) tomograph, which provides precise compositions of the γ- and γ′-phases. Given the narrow range of composition of the γ/γ′ two-phase field in this ternary alloy,

* Corresponding author. E-mail: pbocchin@gmail.com

1359-6462/$ - see front matter © 2012 Acta Materialia Inc. Published by Elsevier Ltd. All rights reserved.
http://dx.doi.org/10.1016/j.scriptamat.2012.11.035

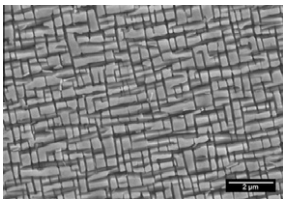

Figure 1. Secondary electron SEM micrograph of etched Co–9.7Al–10.8W aged at 900 °C for 1006 h. The light contrast reveals cuboidal γ′-precipitates, while dark contrast indicates the γ-matrix channels that have been selectively etched.

these precise compositions are essential for alloy manufacturing. Additionally, the subnanometer-level spatial resolution of the LEAP tomograph provides detailed information on partitioning between the two phases and segregation behavior at the matrix/precipitate interface in a Co–Al–W alloy, which has previously been reported for Ni–Cr–Al alloys [11,20].

The alloy was prepared by arc-melting 99.95% Co, 99.999% Al and 99.97% W under argon gas. Cast ingots were homogenized at 1300 °C for 2 h, aged at 900 °C for 1006 h (~42 days) and subsequently quenched in water. The homogenized alloy composition was Co–9.3Al–11.0W, as measured on polished samples by energy-dispersive X-ray spectroscopy (EDS) using a Hitachi[1] field-emission scanning electron microscope (SEM), S4700. Standards for each element were used in the EDS analysis. SEM microstructure imaging was performed on aged samples etched with a solution of 100 ml deionized H_2O, 10 ml of 65% HNO_3, 50 ml of 32% HCl and 10 g of $FeCl_3$. APT specimens were fabricated using an FEI Helios Nanolab microscope, equipped with an electron gun and a Ga focused ion beam (FIB). Three microtips were sharpened with Ga^+ ions to ~50 nm radius, with a final FIB energy of 5 keV at a current of 16 pA. APT measurements were performed with a Cameca 4000X-Si LEAP tomograph with a picosecond ultraviolet (wavelength = 355 nm) laser energy of 30 pJ per pulse, a pulse repetition rate of 200 kHz, a microtip temperature of 35 K, and evaporation rates (ion per pulse) of 3% for microtip 1 and 5% for microtips 2 and 3. These conditions were chosen based on a calibration study of the homogenized Co–9.3Al–11.0W alloy, in which the composition was measured as a function of laser pulse energy, microtip temperature, pulse repetition rate and evaporation rate. During this study it was found that the composition of the homogenized sample as measured by APT was Co–9.65Al–10.77W. All results were analyzed using Cameca's IVAS 3.6.2 APT software.

Figure 1 shows an SEM micrograph of a representative etched cross-section of the alloy. The structure consists of a high volume fraction of γ′ (80 ± 4%) as determined by the line intercept method measured from backscattered SEM micrographs of unetched samples oriented near the

[1] Certain commercial equipment, instruments or materials are identified in this article to foster understanding. Such identification does not imply recommendation or endorsement by the National Institute of Standards and Technology, nor does it imply that the materials or equipment identified are necessarily the best available for the purpose.

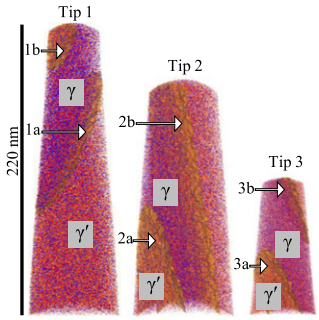

Figure 2. APT three-dimensional reconstructions of microtips 1-3, where the γ/γ′ interfaces are indicated by 8.6 at.% W isoconcentration surfaces. Arrows indicate the six γ/γ′ interfaces present in the microtips. The Co, Al and W atoms are represented in blue, red and orange, respectively. Each spot indicates a single atom. (For interpretation of the references to color in this figure legend, the reader is referred to the web version of this article.)

001-orientation, which is in agreement with the 83 ± 5% calculated from pixel counting image analysis of the same micrographs. Figure 2(a–c) displays APT reconstructions for microtips 1, 2 and 3, which contain 30, 38 and 8 million atoms, respectively. Ga contamination from ion milling was <0.009 at.%. As anticipated (Fig. 1), γ′-precipitates are too large to be fully encompassed in an APT microtip, so the reconstructions exhibit only partial γ′-precipitates. The γ/γ′ interfaces in Figure 2(a–c) are represented by orange 8.6 at.% W isoconcentration surfaces. All microtips contain a γ-channel between two γ′-precipitates imaged partially due to their large size. As anticipated from the SEM image of closely packed cuboidal precipitates (Fig. 1), all γ/γ′ interfaces are planar with the exception of interface 3b in microtip 3, which contains a slight degree of curvature. Subsequent transmission electron microscopy (TEM) on the aged sample revealed a very small amount of μ-phase, which was not observable by SEM analysis. The small volume fraction is unlikely to affect the compositional results of the γ- and γ′-phases.

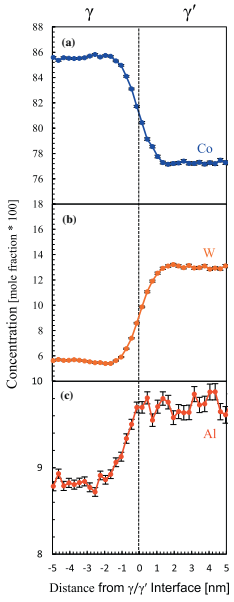

Figure 3. Proximity histograms of the five interfaces displayed in Figure 2, for (top) Co, (middle) W and (bottom) Al.

Table 1. Calculated values of the relative Gibbsian excess, $\Gamma_A^{B,C} = A[B,C]$, and change in interfacial free energy, $\Delta\sigma$, across each interface.

Interface	Relative excess (nm^{-2})			$\Delta\sigma$ ($mJ\ m^{-2}$)		
	Co[Al,W]	W[Co,Al]	Al[Co,W]	Co[Al,W]	W[Co,Al]	Al[Co,W]
1a	-10.76 ± 2.54	-4.18 ± 1.09	0.97 ± 0.23	3.01 ± 0.90	20.66 ± 7.30	-1.11 ± 0.32
1b	8.12 ± 6.48	3.94 ± 3.07	-0.75 ± 0.62	-1.64 ± 2.34	-12.79 ± 21.60	0.49 ± 0.66
2a	-8.922 ± 3.90	-5.31 ± 2.68	-0.832 ± 0.36	2.09 ± 1.10	49.81 ± 18.36	1.01 ± 0.46
2b	-20.76 ± 3.08	-6.76 ± 1.00	1.79 ± 0.26	10.54 ± 3.08	52.43 ± 1.00	-3.66 ± 0.25
3a	1.71 ± 3.46	1.19 ± 2.38	-0.17 ± 0.34	-1.69 ± 0.96	-51.98 ± 59.00	0.67 ± 0.39
3b	-17.14 ± 5.06	6.29 ± 2.20	1.57 ± 0.45	5.61 ± 3.54	-33.16 ± 17.64	-2.03 ± 0.85

Interfacial segregation behavior was measured using the proximity histogram (or proxigram) method [21], which yields concentration profiles. Figure 3 shows interfacial compositions ranging ±5 nm from the γ/γ′ interface, defined by the inflection point of the majority species, Co. The far-field composition of all species deviates from the average by ~0.05–0.2 at.%. The concentration of Al fluctuates more than those of Co and W; this is simply an artifact of the smaller scale of the *y*-axis when compared to the Co and W plots. The partitioning ratios are defined by $k_i = \frac{C_i^{\gamma'}}{C_i^{\gamma}}$, where i = Co, Al or W, which are 0.91, 1.11 and 2.19, respectively. In the Co–Al–W system, W shows greater partitioning behavior than Al. This is unlike in the Ni–Cr–Al system, where the Al partitioning ratio is largest [20]. This difference may be the result of the supersaturation of W being greater than that of Al in the initial γ′-nuclei. For a ternary alloy, the relative Gibbsian interfacial excess is calculated using:

$$\Gamma_A^{B,C} = \Gamma_A - \Gamma_B \frac{c_C^{\gamma} c_A^{\gamma'} - C_A^{\gamma} c_C^{\gamma'}}{c_C^{\gamma} c_B^{\gamma'} - C_B^{\gamma} c_C^{\gamma'}} - \Gamma_C \frac{c_A^{\gamma} c_B^{\gamma'} - C_B^{\gamma} c_A^{\gamma'}}{c_C^{\gamma} c_B^{\gamma'} - C_B^{\gamma} c_C^{\gamma'}} \qquad (1)$$

where $\Gamma_A^{B,C}$ is the Gibbsian interfacial excess of element A relative to elements B and C; Γ_A, Γ_B and Γ_C are the Gibbsian interfacial excesses of elements A, B and C, respectively, and are determined using the proximity histogram method [22]. The variables C_i^{γ} and $C_i^{\gamma'}$ are the concentrations of element i in the γ-matrix and the γ′-precipitates [23,24].

The relative Gibbsian interfacial excess and the reduction of interfacial energy were calculated and are presented in Table 1 [25]. The relative excess values for Co, Al and W at each interface presented in Table 1 vary between negative and positive values, implying that the interfacial composition is continuously changing, which implies, in turn, that the system is not at thermodynamic equilibrium. A positive excess implies a reduction in the interfacial energy, whereas a negative value implies an increase in interfacial energy; this follows from the Gibbs adsorption isotherm, assuming that the solute species obey Henry's law. Specifically, the Gibbs adsorption isotherm for an element A, at constant temperature T, pressure P and chemical potentials μ_i of B and C, is given by

$$\left(\frac{d\sigma}{dc_i}\right)_{T,P,\mu B,\mu C} = -k_B T \Gamma_A^{B,C}$$

where k_B is Boltzmann's constant. The change in σ due to the relative Gibbsian interfacial excess is obtained by integrating $\left(\frac{d\sigma}{dc_i}\right)$ [23,25]. In summary, detailed analyses of the concentration profiles yield three basic physical quantities concerning γ/γ′ interfaces, which are important for understanding the coarsening behavior of γ′-precipitates.

The compositions of each phase were measured in a region of interest (3–6 million atoms for the γ-phase and 13–15 million atoms for the γ′-phase) located at least 10 nm away from the γ/γ′ interface. Results for these measurements are displayed in Table 2. Compositional measurements for the γ-phase were recorded in the three microtips. The composition of the γ′-phase was taken from the large γ′-volume located below the Al interface 1a and above interface 2b in microtips 1 and 2. The compositions of the other γ′-precipitates are not reported because their volume is much smaller than those of the large precipitates from microtips 1

Table 2. Average γ- and γ′-phase compositions measured in this study as compared to the compositions reported by Sato et al. [5] and near-single-phase $L1_2$ structure alloys [16,18].

This study	γ (at.%)			γ′ (at.%)		
	Co	Al	W	Co	Al	W
Co–9.7Al–10.8W						
Tip 1	85.48	8.90	5.61	77.58	9.96	12.49
Tip 2	85.36	8.89	5.75	77.42	10.09	12.46
Tip 3	85.16	9.12	5.72	–	–	–
Average	**85.33 ± 0.16**	**8.9 ± 0.13**	**5.69 ± 0.07**	**77.50 ± 0.11**	**10.03 ± 0.09**	**12.48 ± 0.02**
Sato et al.[a]	85.4	9.2	5.4	78.1	9.9	12.0
Co–9.2Al–9W						
Co–9Al–7.5W	85.5	8.9	5.6	78.7	9.0	12.3
Inui et al.[b] (PC)	–	–	–	77	12	11
Miura et al.[b] (PC)	–	–	–	78	10	12
Inui et al.[b] (SC)	–	–	–	79	10	11

The alloys listed below the bold horizontal line are attempts to produce polycrystalline (PC) and single crystal (SC) single-phase γ′ ingots.

[a] Data reported graphically in the phase diagram; the diameter of symbol implies an error bar of ±0.5 at.%. Neither compositions nor their errors are reported explicitly by Sato et al. [5].

[b] The values reported are the nominal alloy compositions of attempted castings of single-phase γ′-alloys.

and 2, which gave rise to fluctuations in composition due to the small number of atoms in those precipitates.

In Figure 4, our γ- and γ′-compositional measurements are superimposed on the Sato et al. phase diagram, which measured phase compositions on two alloy cross-sections by field-emission electron-probe microanalysis (FE-EPMA). Our γ-composition, measured by LEAP tomography, is in excellent agreement with the FE-EPMA results. The LEAP tomographic composition for the γ′-phase is, however, slightly richer in W and Al (by ~0.5 and 0.1 at.%, respectively, which is close to the statistical uncertainty in the Al concentration); the γ′-phase is leaner in Co (by ~0.5 at.%) than the upper γ′-solvus curve of the Co–9.2Al–9W alloy. Sato et al. aged their Co–9.2Al–9W and Co–9Al–7.5W alloys for 72 h at 900 °C, while we used a much longer aging time, ~1000 h, for an alloy richer in W (Co–9.7Al–10.8W) and thus with the larger γ′-volume fraction. The discrepancy in the location of the γ′-solvus curve indicates that equilibrium had not been achieved for Sato et al.'s 72 h treatment. The small magnitude of this discrepancy, for alloys aged for 72 and 1006 h, indicates that after 1006 h our specimens are nearer their equilibrium γ- and γ′-concentrations. Longer aging times are needed to confirm this hypothesis.

In summary, atomic partitioning coefficients, segregation behavior and the reduction in the interfacial free energy of the γ/γ′ phase interfaces of a Co–9.7Al–10.8W superalloy aged at 900 °C for 1006 h have been measured using APT. The γ-phase matrix composition, as measured by LEAP tomographic analyses, agrees well with the FE-EPMA measurements reported for W-leaner specimens (Co–9.2Al–9W and Co–9Al–7.5W) aged at 900 °C for a shorter time, 72 h, while the γ′-phase composition exhibits somewhat higher concentrations of W and Al (~0.5 and 0.1 at.%, respectively) and lower Co concentrations (by ~0.5 at.%) [5]. The close agreement in the γ- and γ′-compositions between the two studies (aging times of 72 and 1006 h) indicates that the phase compositions are close to their equilibrium values, but this must be confirmed by additional experiments on specimens aged for longer times.

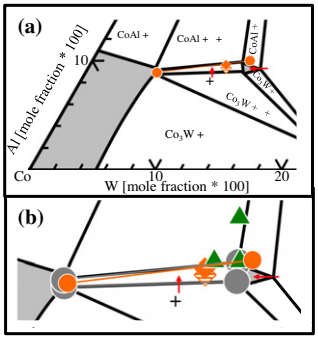

Figure 4. Co–Al–W phase diagram at 900 C published by Sato et al. [5], (a) with compositions of the γ- and γ′-phases, as measured in this study (orange dots), as well as (b) the compositions of the near-single-phase $L1_2$ structure taken from Sato et al. [5] (grey) and literature [16–18] values (green). The solid orange diamond marks the nominal composition as measured by APT, while the orange striped diamond indicates the composition as measured by EDS. (For interpretation of the references to color in this figure legend, the reader is referred to the web version of this article.)

This research was sponsored by the US Department of Energy, Office of Basic Energy Sciences (Dr. John Vetrano, monitor) through Grant DE-FG02-98ER45721. P.J.B. received partial support from the NASA Aeronautics Scholarship Program. APT measurements were conducted at the Northwestern University Center for Atom-Probe Tomography (NUCAPT). The LEAP tomograph was purchased with funds from the NSF-MRI Program through Grant DMR 0420532 (Dr. Charles Bouldin, monitor) and from the ONR-DURIP Program through Grant N00014-0400798 (Dr. Julie Christodoulou, monitor). The authors would like to thank Dr. D. Isheim for managing NUCAPT and Drs. I. Blum and J. Saal for valuable discussions. We also gratefully acknowledge the Initiative for Sustainability and Energy at Northwestern (ISEN) for Grants to upgrade the capabilities of NUCAPT.

[1] C.T. Sims, N.S. Stoloff, W.C. Hagel, Superalloys II, John Wiley & Sons Inc., New York, 1987.
[2] M. Durand-Charre, The Microstructure of Superalloys, Gordon & Breach Science Publishers, Amsterdam, 1997.
[3] M. McLean, G. Webster, F. Nabarro, A. Cottrell, Philos. Trans. R. Soc. Lond. A 351 (1995) 419.
[4] R.C. Reed, The Superalloys: Fundamentals and Applications, Cambridge University Press, Cambridge, 2006.
[5] J. Sato, T. Omori, K. Oikawa, I. Ohnuma, R. Kainuma, K. Ishida, Science 312 (2006) 90.
[6] A. Suzuki, G. Denolf, T. Pollock, Scripta Mater. 56 (2007) 385.
[7] A. Suzuki, T.M. Pollock, Acta Mater. 56 (2008) 1288.
[8] A. Bauer, S. Neumeier, F. Pyczak, M. Goken, Scripta Mater. 63 (2010) 1197.
[9] A. Bauer, S. Neumeier, F. Pyczak, R.F. Singer, M. Goken, Mater. Sci. Eng. A 550 (2012) 333.
[10] M.S. Titus, A. Suzuki, T.M. Pollock, Scripta Mater. 66 (2012) 574.
[11] C. Booth-Morrison, J. Weninger, C.K. Sudbrack, Z. Mao, R.D. Noebe, D.N. Seidman, Acta Mater. 56 (2008) 3422.
[12] Z. Mao, C. Booth-Morrison, C.K. Sudbrack, G. Martin, D.N. Seidman, Acta Mater. 60 (2012) 1871.
[13] Y. Tsukamoto, S. Kobayashi, T. Takasugi, Mater. Sci. Forum 654–656 (2010) 448.
[14] S. Kobayashi, Y. Tsukamoto, T. Takasugi, H. Chinen, T. Omori, K. Ishida, S. Zaefferer, Intermetallics 17 (2009) 1085.
[15] K. Tanaka, T. Ohashi, K. Kishida, H. Inui, Appl. Phys. Lett. 91 (2007) 181907.
[16] S. Miura, K. Ohkubo, T. Mohri, Mater. Trans., JIM 9 (2007) 2403.
[17] N.L. Okamoto, T. Oohashi, H. Adachi, K. Kishida, H. Inui, P. Veyssiére, Philos. Mag. A 91 (2011) 3667.
[18] H. Inui, T. Oohashi, N.L. Okamoto, K. Kishida, K. Tanaka, Adv. Mater. Res. 278 (2011) 1.
[19] S. Meher, H.-Y. Yan, S. Nag, D. Dye, R. Banerjee, Scripta Mater. 67 (2012) 850.
[20] C.K. Sudbrack, K.E. Yoon, R.D. Noebe, D.N. Seidman, Acta Mater. 54 (2006) 3199.
[21] O.C. Hellman, J.A. Vandenbroucke, J. Rusing, D. Isheim, D.N. Seidman, Microsc. Microanal. 6 (2000) 437.
[22] O.C. Hellman, J. Rusing, J.T. Sebastian, D.N. Seidman, Mater. Sci. Eng. C: Biomimetic Supramol. Syst. 15 (2001) 13–15.
[23] A. Biswas, D.J. Siegel, C. Wolverton, D.N. Seidman, Acta Mater. 59 (2011) 6187–6204.
[24] S.A. Dregia, P. Wynblatt, Acta Metall. Mater. 39 (1991) 771–778.
[25] I.D. Blum, S. Baik, M.G. Kanatzidis, D.N. Seidman, unpublished manuscript.